Application of interval field method to the stability analysis of slopes in presence of uncertainties

Chengxin Feng[a], Matthias Faes[b], Matteo Broggi[a,*], Chao Dang[a], Jiashu Yang[a,e], Zhibao Zheng[c], Michael Beer[a,d,e,f]

[a] *Institute for Risk and Reliability, Leibniz University Hannover, Callinstr. 34, 30167 Hannover, Germany*
[b] *TU Dortmund University, Chair for Reliability Engineering, Leonhard-Euler-Strasse 5, 44227 Dortmund.*
[c] *Institute of Mechanics and Computational Mechanics, Leibniz University Hannover, Appelstraβe 9a, 30167 Hannover, Germany*
[d] *Institute for Risk and Uncertainty and School of Engineering, University of Liverpool, Liverpool L69 7ZF, UK*
[e] *International Joint Research Center for Engineering Reliability and Stochastic Mechanics, Tongji University, Shanghai 200092, PR China*
[f] *International Joint Research Center for Resilient Infrastructure, Tongji University, Shanghai 200092, PR China*

Abstract

Spatial uncertainty of soil parameters has a significant impact on the analysis of slope stability. Interval field analysis is emerging as a complementary tool of the conventional random field method that can take spatial uncertainty into account, which, however, has not been investigated in slope stability analysis. The present paper proposes a new method, named the interval field limit equilibrium method (IFLEM), for assessing the stability of slope in the presence of the interval field. In this method, the modified exponential function is introduced to characterize the spatial uncertainty of the interval field and the Karhunen-Loève-like decomposition is employed to generate the interval field. Then, in a single calculation, the deterministic slope stability analyzed by the Morgenstern-Price approach is implemented in order to estimate the safety factor. Subsequently, the upper and lower bounds of the interval of safety factor are efficiently evaluated by a kind of surrogate-assisted global optimization algorithms, such as Bayesian global optimization used in this study. Finally, the effectiveness of the proposed method is verified by two numerical examples. The results indicate that the proposed method can provide reasonable accuracy and efficiency, which is potentially applicable to a number of geotechnical systems.

Keywords: Spatial uncertainty, Interval field, Spatial dependency function, Karhunen-Loève like expansion, Slope stability

---

*Corresponding author: broggi@irz.uni-hannover.de

1. Introduction

Slope failure is a major threat to people's lives and property in mountainous areas. Due to the complex material composition and various deposition conditions, there is considerable spatial uncertainty in the properties of geotechnical materials (Phoon and Kulhawy, 1999a). Previous studies have indicated that the spatial uncertainty usually has a great impact on the design and analysis of geotechnical structures, hence it should be properly taken into account (Länsivaara et al., 2021). The random field theory as one of the feasible techniques to characterize the spatial uncertainty (Phoon and Kulhawy, 1999b; Griffiths and Fenton, 2004). A series of progresses have been emerged in recent decades, particularly a comprehensive overview is given (Jiang et al., 2022). Although the random field theory can address the spatial uncertainties, it requires a large number of samples to obtain statistical characteristics, such as mean value, coefficient of variation, and correlation function. However, it is difficult to estimate these parameters in the presence of sparse measurement data, particularly the correlation length and correlation function (Cami et al., 2020). To address the challenges connected to the statistical inference of the properties of autocorrelation functions, Wang et al. (2019) proposed a bootstrap method for statistically inferring the autocorrelation coefficients as well other parameters of a random field. However, for sparsely sampled random fields, extra statistical uncertainties are introduced when estimating the sampling distribution of the random field parameters (Montoya-Noguera et al., 2019).

Alternatively to random fields, the interval field method proposed by (Moens et al., 2011) only requires the upper and lower bounds of material parameters, as well as a description of the spatial dependence for modelling the spatial information. These characteristics of interval fields are particularly desirable in cases where statistical data are lacking (Beer et al., 2013; Faes and Moens, 2019). This method represents the uncertainty of bounded parameters that vary in time or space as a series of deterministic basis functions multiplied by a superposition of interval factors. So far, a number of scholars have promoted the interval field method in different fields. Faes and Moens (2017, 2020a) presented a novel methodology for the identification and quantification of spatial uncertainty modelled as an interval field, including potential cross-dependence. Sofi et al. (2015, 2019) introduced an interval finite element method which incorporates the interval field representation of uncertainties by applying an interval extension in conjunction with the standard energy approach. Ni and Jiang (2020); Ni et al. (2016) proposed an interval field model to represent spatial uncertainties with insufficient information, in which the variation of the parameters at each location is quantified by an interval with upper and lower bounds. Callens et al. (2021) presented a method to model local explicit interval fields, which are less computationally demanding and less conservative than global explicit interval fields.

It can be seen that the interval field method is receiving growing attention, but its application in geotechnical engineering is rarely reported. Therefore, the present study expands its scope on characterizing the spatial uncertainty in geotechnical engineering.

In practical terms, an interval field can be regarded as a family of dependent interval variables indexed by location. When considering this interpretation, the methods developed for propagating interval variables could also be applicable to the propagation of interval fields. Over the past several decades, a plethora of methods have been developed for interval uncertainty propagation, such as the interval arithmetic (Moens and Hanss, 2011), the interval perturbation methods (Wang et al., 2014) and the global optimization approach (Deng et al., 2017), etc. It is recommended to refer to (Faes and Moens, 2020b) for a comprehensive review on the related computational methods. Among these algorithms, global optimization approaches are the standard technique for solving interval problems. The main downside is the computational effort of these approaches. To reduce the computational efforts required by heuristic global optimization algorithms (e.g., genetic algorithm), Kriging-assisted global optimization techniques have been investigated in the context of interval uncertainty propagation (Catallo, 2004). In this direction, a Bayesian global optimization is also presented to obtain the lower and upper response bounds of a computationally expansive model subject to multiple interval variables (Dang et al., 2022).

In this paper, the stability analysis of slopes is analyzed when the spatial uncertainty affecting the slopes is modeled by interval fields. The main contributions of this work are summarized as follows: first, the interval field is introduced to characterize the spatial uncertainty of slopes. This is a modelling strategy complementary to the conventionally used random fields, and it is, to the authors' best knowledge, applied to slope stability for the first time. In this representation, an expansion over an orthogonal basis, similar to the Karhunen-Loève-like decomposition in random field analysis, is used to represent the interval field by employing multiple interval variables. Second, a general methodology, called the interval field limit equilibrium method (IFLEM), is proposed to propagate interval fields in slopes. This approach estimates the resulting lower and upper bounds of the safety factor of the slope stability. Additionally, the Bayesian global optimization algorithm is applied to find the lower and upper bounds of the safety factor of a slope characterized by multiple interval variables, where the Morgenstern-Price method is employed for deterministic analysis.

The rest of this paper is arranged as follows: section 2 introduces the basic knowledge of the interval field, and section 3 incorporates the methodology that will be used in this paper. Section 4 illustrates the procedure of the interval field limit equilibrium method. Two numerical examples are given to demonstrate the effectiveness of the interval field limit equilibrium method in section 5, and conclusions are drawn in section 6.

2. Interval field theory

An interval field can be understood as a set of dependent intervals indexed by the location throughout the model domain and/or time. The interval field model solves the problems of changing mechanical parameters with spatial location from a non-probabilistic perspective by measuring the spatial uncertainty of the parameters in the form of upper and lower bounds (Sofi et al., 2019). Specifically, the represent interval fields are based on spatial dependence functions and Karhunen-Loéve (K-L) like expansions. The spatial dependence function is adopted to represent the dependence of interval variables in different spatial positions. In addition, the specific expansion form of the interval fields can be obtained through the K-L like series expansion.

2.1. Interval field expansion

In probability theory, random fields are generally used to quantify the uncertainty of a spatially uncertain parameter, in which the quantity at arbitrary location $\mathbf{x} \in \Omega \subset \mathbb{R}^{n_{\mathrm{d}}}$ is considered as a random variable with a probability distribution, where $\mathbf{x}$ is the spatial coordinate in n_{d} dimensions in the physical model domain Ω. Different from the random field model, the interval field model employs bounds, namely a pair of upper and lower bounds, to describe the spatial uncertainty, which can efficiently perform uncertainty analysis based on limited information (Chen et al., 2020). For specific problems, how to represent the interval field is the basis of simulation calculations. In this paper, the K-L like expansion is used to represent the interval field $\psi^I(\mathbf{x}) : \Omega \times \mathbb{IR} \mapsto \mathbb{IR}$, with $\mathbb{IR}$ the space of interval valued real numbers. The expansion of an interval field is written as:

$$\psi^I(\mathbf{x}) = \psi_{\mathrm{o}}^I(1 + \psi_n^I(\mathbf{x})), \tag{1}$$

$$\psi_n^I(\mathbf{x}) = \sum_{j=1}^{\infty} \sqrt{\lambda_j} f_j(\mathbf{x}) \zeta_j, \tag{2}$$

where ψ_{o}^I is the center value of the interval field, $\psi_n^I(\mathbf{x})$ is a dimensionless interval field with unit range, $\lambda_m \in [0, \infty)$ is the m-th eigenvalue of the spatial dependency function, $f_m : \Omega \mapsto \mathbb{R}$ is the m-th eigenfunction of the spatial dependency function, and $\zeta_j \in \mathbb{IR}$ is the j-th extra unitary interval (Sofi, 2015).

The extra unitary interval is quite different from the classical unitary interval. It relies on the rules of the classical interval analysis. The specific details about the classical interval analysis can be found in (Sofi, 2015). The extra unitary interval is given by

$$\zeta_j \in [-1, 1],\ j = 1, 2, \cdots, l. \tag{3}$$

Besides, the uncertain flexibility of the spatial dependency condition is described by a single interval variable constant over the whole range (Sofi, 2015). For that, the following equality holds

$$\zeta_j \times \zeta_j = [0, 1]. \tag{4}$$

For numerical implementation, the interval field is represented by l-term expansions. To be specific, the l-term expansions of the interval field reads

$$\psi^I(\mathbf{x}) = \psi_{\mathrm{o}}^I(1 + \sum_{j=1}^{l} \sqrt{\lambda_j} f_j(\mathbf{x}) \zeta_j). \tag{5}$$

For details of the method, the reader is referred to the work of Sofi et al. (2019). In this process, the error of the l-term expansions of the interval field can be represented as:

$$\varepsilon_{\mathrm{t}}(\psi^I(\mathbf{x})) = 1 - \frac{\sum_{j=1}^{l} \lambda_j}{\sum_{j=1}^{\infty} \lambda_j}, \tag{6}$$

where $\varepsilon_{\mathrm{t}} \in [0, \infty)$ is the error of the l-term expansions of the interval field, λ_j is j-th eigenvalue.

2.2. Spatial dependency function

The key idea behind the interval field model is to describe the spatial dependency of the uncertain property by introducing a real, deterministic, symmetric, non-negative function $\gamma(\mu, \upsilon)$. In analogy with the auto-correlation function characterizing a random field, the analytic expression of $\gamma(\mu, \upsilon)$ needs to be assumed in a consistent way with the engineering information (Sofi, 2015). That is to say, each realization of the interval field may vary arbitrarily within the upper and lower bounds, as sketched in Fig. 1. In this figure, we assumed for simplicity that the upper and lower bounds are constant. The function $\gamma(\mu, \upsilon)$ reflects the dependency between values of the interval field at different locations. Therefore, the $\gamma(\mu, \upsilon)$ is used to characterize spatial uncertainty and has a number of formulations, such as the single exponential model, squared exponential model, etc (Cami et al., 2020). Among them, the modified exponential model is differentiable at the origin, such that the K-L expansion itself exhibits higher computational efficiency (Spanos et al., 2007; Faes et al., 2022). Thus, in this paper, we assumed that the spatial dependency function, $\gamma(\mu, \mu', \upsilon, \upsilon')$, has the following modified exponential form:

$$\gamma(\mu, \mu', \upsilon, \upsilon') = \exp\left(-\frac{|\mu - \mu'|}{l_{\mathrm{h}}} - \frac{|\upsilon - \upsilon'|}{l_{\mathrm{v}}}\right)(1 + \frac{|\mu - \mu'|}{l_{\mathrm{h}}})(1 + \frac{|\upsilon - \upsilon'|}{l_{\mathrm{v}}}), \tag{7}$$

where $\gamma(\mu, \mu', \upsilon, \upsilon')$ is the spatial dependency function, (μ, υ) and (μ', υ') denote two points in a 2-D space, $\exp(\cdot)$ is the exponential function, l_{h} is the horizontal spatial dependency length which is similar to the horizontal correlation distance, l_{v} is the vertical spatial dependency length which is similar to the vertical correlation distance, $|\mu - \mu'|$ and $|\upsilon - \upsilon'|$ respectively denote the horizontal and vertical distances between the two points.

In this paper, an assumed spatial dependency function, the modified exponential function is used for illustrative purpose. After the spatial dependency function $\gamma(\mu, \mu', \upsilon, \upsilon') : \Omega \times \Omega \mapsto \mathbb{R}$ is determined, the

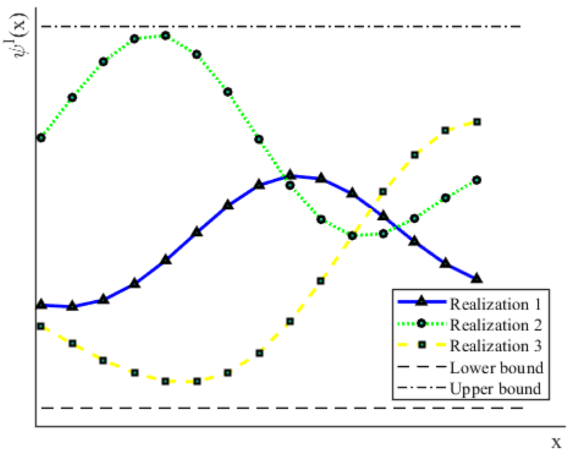

Fig. 1. Sketch of the interval field

spatial uncertainty can then be characterized (Faes et al., 2022). Specifically, the Fredholm integral equation of the second kind is solved to obtain the eigenvalues and eigenfunctions of the $\gamma(\mu, \mu', \upsilon, \upsilon')$ (Atkinson and Han, 2009). The Fredholm integral equation of the second kind takes the form:

$$\int_{\Omega} \gamma(\mu, \mu', \upsilon, \upsilon') f_j(\mu', \upsilon') \mathrm{d}\mu' \mathrm{d}\upsilon' = \lambda_j f_j(\mu, \upsilon), \tag{8}$$

where λ_j is the j-th eigenvalue of the spatial dependency function, and $f_j(\cdot)$ is the j-th eigenfunction of the spatial dependency function. In order to numerically solve the Fredholm integral equation of the second kind, the interval field is first discretized into a series of points, and the integral Eq. (8) is solved by determining the eigenvalues and eigenvectors of the covariance matrix.

3. Interval field limit equilibrium method

In this section, the fundamental knowledge and computational formula of the proposed interval field limit equilibrium method are introduced. First, a limit equilibrium method, namely the Morgenstern-Price method, is introduced to calculate the safety factor of the slope with the interval field of cohesion and internal friction angle. Then, the Bayesian global optimization is elaborated to calculate the upper and lower bounds of the safety factor of this slope.

3.1. *Limit equilibrium method and its extension to interval field*

This subsection first introduces the limit equilibrium method for slope stability analysis. Then the extension of the interval field into the limit equilibrium method is studied.

3.1.1. *Limit Equilibrium Method*

Soil slope stability analysis refers to the analysis of the mutual balance between sliding factors and resistance factors on the sliding surface of a soil slope. Soil slope has the tendency to move downward and outward under the action of gravity and other external forces, if the soil inside the slope can resist this tendency, then the slope is stable, otherwise sliding will occur (Liu et al., 2015).

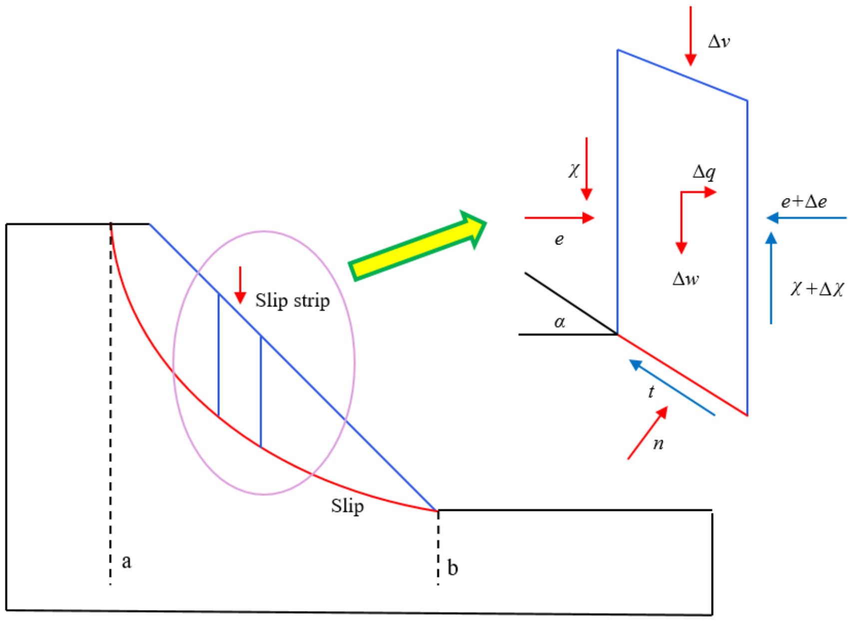

Fig. 2. Schematic diagram of limit equilibrium method

The limit equilibrium method (LEM) used in this paper is the Morgenstern-Price method. The Morgenstern-Price method is similar to the Spencer method, but it allows for various user-specified interslice force functions (Morgenstern and Price, 1965). In the Morgenstern-Price method, it is assumed that

$$\chi_1/e_1 = \tan\beta = \lambda f(u), \tag{9}$$

where χ_1 is inter-slice vertical force, e_1 is inter-slice horizontal force, λ is a constant, and f is an inter-slice function. In particular, the inter-slice functions in the present implementation is half-sine function.

According to Fig. 2, the equilibrium equations of the forces in the horizontal and vertical directions are derived respectively. The obtained equations are shown as follows:

$$t \sin \alpha + n \cos \alpha = \Delta w + \Delta v - \Delta \chi, \tag{10}$$

$$t \cos \alpha - n \sin \alpha = \Delta q - \Delta e, \tag{11}$$

$$t \cos \alpha = c \Delta \chi \sec \alpha + n \tan \varphi, \tag{12}$$

where t is tangential force at the bottom of the soil strip, n is the normal force at the bottom of the soil strip, α is the angle between the tangent line at the bottom of the soil strip and the horizontal direction, Δw is the gravity of the soil strip, Δv is the external force on the soil strip in the vertical direction, $\Delta \chi$ is the difference in vertical force between strips on both sides of the soil strip, Δq is the horizontal component of the soil strip, Δe is the difference in horizontal force between strips on both sides of the soil strip, c is cohesion, and φ is internal friction angle.

In addition, the equilibrium equation of the moment is derived as follows

$$(\chi + \Delta \chi) \frac{\Delta p}{2} + \chi \frac{\Delta p}{2} + (e + \Delta e) \Delta q - e \Delta r - \Delta q \Delta s = 0, \tag{13}$$

where χ is the lower soil bar which is subjected to the inter-slice vertical force of the upper soil bar, Δp is the width of the soil strip, e is the lower soil strip is subjected to the horizontal force between the strips of the upper soil strip, Δq is the distance between the position of the force of the lower soil strip on the upper soil strip and the center point of the bottom of the strip, Δr is the distance between the position of the force of the upper soil strip on the lower soil strip and the center point of the bottom of the strip, and Δs is the distance between the position of the horizontal component of the soil strip and the center of the bottom of the strip.

Based on the theory of the limiting equilibrium method, the safety factor (f_{s}) of the slope can be obtained by equilibrium conditions (Zhu et al., 2005). The f_{s} of the slope can be calculated from Eqs. (14) and (15) by combining Eqs. (10)-(13) according to the equilibrium condition of force and moment, that is,

$$-\frac{\mathrm{d}e}{\mathrm{d}p}(1+\tan\varphi\tan\alpha)+\frac{\mathrm{d}\chi}{\mathrm{d}p}(\tan\varphi-\tan\alpha)=c\sec^2\alpha+\left(\frac{\mathrm{d}w}{\mathrm{d}p}+\frac{\mathrm{d}v}{\mathrm{d}p}\right)$$
$$(\tan\varphi-\tan\alpha)-\frac{\mathrm{d}q}{\mathrm{d}p}(1+\tan\varphi\tan\alpha), \tag{14}$$

$$\int_a^b [\lambda f(p)e - e\tan\alpha]\ \mathrm{d}p=\int_a^b \frac{\mathrm{d}q}{\mathrm{d}p}\Delta s\ \mathrm{d}p. \tag{15}$$

3.1.2. Extension to interval field

The equilibrium equation of the force is first established. In the process, cohesion and internal friction angle are expressed in the form of interval fields. Then the equilibrium equation of the moments is established. Finally, the equilibrium formulas for the forces and moments are combined to calculate the f_{s} for the slope. The equilibrium equation of the force is

$$t\cos\alpha=\psi_c^I\Delta p\sec\alpha+n\tan\psi_\varphi^I, \tag{16}$$

where t is the tangential force at the bottom of the soil strip, α is the angle between the tangent line at the bottom of the soil strip and the horizontal direction, ψ_c^I is the interval field of c, and ψ_φ^I is the interval field of φ.

Combining the equilibrium equations of force and moment yields the equation of the interval field limit equilibrium method. Specifically, it is written as

$$-\frac{\mathrm{d}e}{\mathrm{d}p}(1+\tan\psi_\varphi^I\tan\alpha)+\frac{\mathrm{d}\chi}{\mathrm{d}p}(\tan\psi_\varphi^I-\tan\alpha)=\psi_c^I\sec^2\alpha+(\frac{\mathrm{d}w}{\mathrm{d}p}+\frac{\mathrm{d}v}{\mathrm{d}p})$$
$$(\tan\psi_\varphi^I-\tan\alpha)-\frac{\mathrm{d}q}{\mathrm{d}p}(1+\tan\psi_\varphi^I\tan\alpha), \tag{17}$$

where ψ_c^I is interval field of c, ψ_φ^I is interval field of φ, χ is the lower soil bar is subjected to the interbar vertical force of the upper soil bar, and e is the lower soil strip is subjected to the horizontal force between the strips of the upper soil strip.

3.2. Estimate the safety factor bounds by Bayesian global optimization

With the development of optimization methods, surrogate models have evolved into methods that incorporate new data points based on historical data and approximate the global optimal solution, i.e., Bayesian global optimization (Jones et al., 1998; Han and Görtz, 2012). In this problem, the optimization problem can be formulated as

$$\begin{cases} \max \; f_{\mathrm{s}}(\boldsymbol{\zeta}) \\ \min \; f_{\mathrm{s}}(\boldsymbol{\zeta}) \\ \text{s.t. } \zeta_j \times \zeta_j = [0,1], \end{cases} \tag{18}$$

where $\boldsymbol{\zeta} = (\zeta_1, \zeta_2, \cdots, \zeta_l)^{\mathsf{T}}$ is the l-dimensional vector of interval variables, $f_{\mathrm{s}}(\boldsymbol{\zeta}) : \mathbb{IR}^l \mapsto \mathbb{IR}$ is the objective function, and $\zeta_j \times \zeta_j = [0,1]$ is the constraint conditions.

Bayesian global optimization is a black-box optimization algorithm for solving optimization problems for functions with unknown expressions. The algorithm predicts the probability distribution of the function values at any point based on the function values at a set of sampled points, which is achieved by Gaussian process regression. In this subsection, a Bayesian global optimization method that can simultaneously find the minimum and maximum values of the objective function is introduced (Dang et al., 2022). The formula for calculating the minimum value is exhibited in this section. The maximum value is calculated in a similar way after the minimum value is obtained. From the results of the Gaussian process regression, an acquisition function is constructed to measure whether another point is needed to be added, and the extreme value of the acquisition function is solved to determine the next sampling point. In the paper, Bayesian global optimization is used to obtain the intervals of f_{s}.

3.2.1. Initial sample selection

The first step of the optimization algorithm is to select the initial sample points. In the present implementation, the initial samples are uniform random samples inside the unit hyper-sphere (Rubinstein and Kroese, 2016). Then, the initial surrogate model is built based on the initial samples and the associated function values. The Gaussian process regression $\mathcal{N}[\hat{\gamma}(\boldsymbol{\zeta}), s(\boldsymbol{\zeta})]$ is used as a surrogate model, in which $\mathcal{N}[\cdot,\cdot]$ is a normal distribution, $\hat{\gamma}(\boldsymbol{\zeta})$ and $s(\boldsymbol{\zeta})$ are mean value and standard value of predict model respectively. It's performed using the fitrgp function in MATLAB.

3.2.2. Training dataset enrichment

For the minimization problem, the objective function improvement $\theta(\boldsymbol{\zeta})$ is defined as

$$\theta(\boldsymbol{\zeta}) = \max\{\gamma_{\min} - \hat{\gamma}(\boldsymbol{\zeta}), 0\}, \tag{19}$$

where $\gamma_{\min}$ is the current optimal objective function value, and $\hat{\gamma}(\boldsymbol{\zeta})$ is the set of parameters that obey normal distribution.

The expectation value of $\theta(\boldsymbol{\zeta})$ is given by (Jones et al., 1998)

$$\mathbb{E}[\theta(\boldsymbol{\zeta})] = \begin{cases} (\gamma_{\min} - \hat{\gamma}(\boldsymbol{\zeta}))\Phi(\frac{\gamma_{\min} - \hat{\gamma}(\boldsymbol{\zeta})}{s(\boldsymbol{\zeta})}) + s(\boldsymbol{\zeta})\phi(\frac{\gamma_{\min} - \hat{\gamma}(\boldsymbol{\zeta})}{s(\boldsymbol{\zeta})}), s > 0 \\ 0, s = 0, \end{cases} \tag{20}$$

where $\mathbb{E}[\cdot]$ is the expectation operator, Φ is the standard normal cumulative distribution function, ϕ is the standard normal distribution probability density function, $\hat{\gamma}(\boldsymbol{\zeta})$ and $s(\boldsymbol{\zeta})$ are the mean and standard deviation of the normal distribution of the Kriging model predictions, respectively.

The new sample points are found by solving the following suboptimization problem which maximize the value of $\mathbb{E}[\theta(\boldsymbol{\zeta})]$:

$$\begin{cases} \max_{\boldsymbol{\zeta}} \mathbb{E}[\theta(\boldsymbol{\zeta})] \\ \text{s.t. } \zeta_j \times \zeta_j = [0, 1]. \end{cases} \tag{21}$$

3.2.3. Convergence criterion for Bayesian global optimization

The convergence criterion is an essential element for the optimization algorithm. It is determined by controlling the ratio of the maximum expected value of $\theta(\boldsymbol{\zeta})$ to the current optimal objective function value. The convergence criterion of the present paper is defined as

$$\frac{|\max \mathbb{E}[\theta(\boldsymbol{\zeta})]|}{|\gamma_{\min}| + \delta} \leq \epsilon, \tag{22}$$

where $\max\ \mathbb{E}[\theta(\boldsymbol{\zeta})]$ represents the maximum value of $\mathbb{E}[\theta(\boldsymbol{\zeta})]$, $\gamma_{\min}$ represents the minimum value of γ observed so far, δ is an extreme small positive value, ϵ is the threshold value. In this case, δ is 1e-6 and ϵ is 0.001. The optimization process is terminated when the ratio of the maximum expected value of $\theta(\boldsymbol{\zeta})$ to the current optimal objective function value is less than ϵ for three successive iterations.

4. Implementation procedure of IFLEM

By combining the limit equilibrium method, the interval field model, and Bayesian global optimization method, IFLEM is proposed to efficiently estimate the upper and lower bounds of the f_s of a slope. The basic procedure for the numerical implementation of the proposed method (shown in Fig. 3) includes the following five steps:

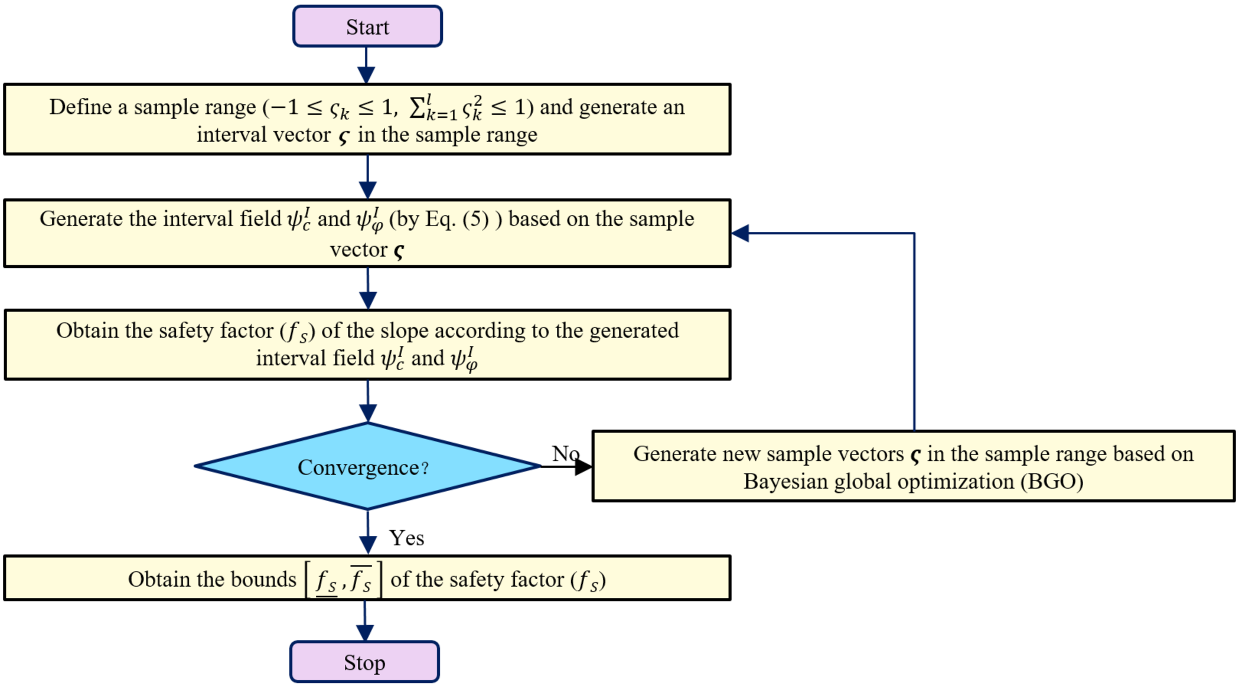

Fig. 3. Flowchart of the proposed IFLEM method

1. An initial sample points are first generated as a scattering set of samples by the method in Section 3.2. The interval field is generated from Eq. (1) based on the selected interval vector.
2. The parameters of the interval field are input into the slope model. The f_s of the slope is evaluated by Eq. (17) according to the interval fields of c and φ.
3. Select the vector samples required for the next calculation according to the optimal additive point criterion by Eq. (19).
4. Determine the termination condition of the optimization by Eq. (22). If the condition is satisfied, the upper and lower bounds of the f_s are obtained according to the calculation. Otherwise, additional

points are required and steps (2) to (4) are repeated until the condition is satisfied.

5. After calculating the f_s, the stability of the slope is evaluated. If the minimum value of the f_s is greater than 1, the slope is in a totally safe state. If the maximum value of the f_s is less than 1, the slope is in a high risk state. If 1 is within the interval of the f_s, the stability of the slope is unsure.

5. Illustrative examples

In order to demonstrate the accuracy and effectiveness of the proposed method, two examples are shown in this section. The first one is a one-stage slope and the second one is a two-stage slope. The purpose of the first case is to show the accuracy and efficiency of this approach. The second one is to show that this method applies to complex problems.

5.1. Example 1: Interval field analysis of a single-stage slope

5.1.1. Description of the problem

To illustrate, a single-stage slope is used to demonstrate the generation of the interval field, and then the interval of the f_s is calculated according to the proposed method. This slope has a height of 28 m and an angle of 36.9°, in which the height of the lower floor is 4 m and the height of the upper floor is 24 m, as shown in Fig. 4. In order to generate interval fields for the slope, 489 elements are discrete in the slope. In the process, the c and φ are spatially variable described by the interval fields which are generated by the method mentioned in Section 2. And we use the parameter of midpoint of the element on behalf of the whole element. The minimum value of c is 15 kPa and the maximum value is 21 kPa, and the minimum value of φ is 16° and the maximum value is 24°. The horizontal spatial dependency length is set to 30 m, and the vertical spatial dependency length is 4 m. The parameters of the slope are shown in Table 1.

5.1.2. Interval field analysis results and discussion

First, the interval field of the single-stage slope is generated and the error of the K-L like expansion level is analyzed. In this example, the error of the K-L like expansion is controlled within 5% and the K-L like expansion term is six (Huang et al., 2001). Then, the eigenfunctions and eigenvalues are solved according

Table 1

Material parameters of the single-stage slope in Example 1

Parameters	Maximum value	Minimum value	l_h	l_v
c(kPa)	21	15	30	4
φ(°)	24	16	30	4

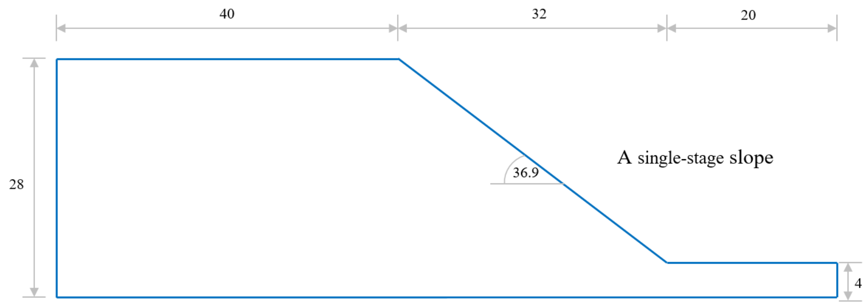

Fig. 4. The geometry model of the single-stage slope

to the spatial dependency function in Section 2. The eigenfunctions are shown in Fig. 5 and the eigenvalues are shown in Fig. 6.

The single-stage slope with interval field is calculated and its sliding surfaces (SS) are obtained as shown in Fig. 7. To calculate the f_s, the sliding surfaces should be selected first. For illustration purposes, three typical sliding surfaces are considered. In this figure, three special sliding surfaces are marked according to the range of the f_s. The red sliding surface in the diagram represents the most dangerous sliding surface, while the green sliding surface represents the safest sliding surface. Each sliding surface was analyzed respectively. The safety factor bounds of the upper and lower of the single-stage slope with interval field are calculated by the Bayesian global optimization method. The interval of f_s was obtained as [0.83, 0.994] for the sliding surfaces 1, [0.946, 1.132] for the sliding surfaces 2, and [1.107, 1.415] for the sliding surfaces 3. The calculated interval of f_s is represented in Fig. 8. The optimization of the sliding surface 1 to obtain the interval of f_s required 19 deterministic analyses, the sliding surface 2 required 20 times, and the sliding surface 3 required 21 times. In Table 2, the results of the Bayesian global optimization are compared with the surrogate optimization method. It can be found that Bayesian global optimization shows great advantages

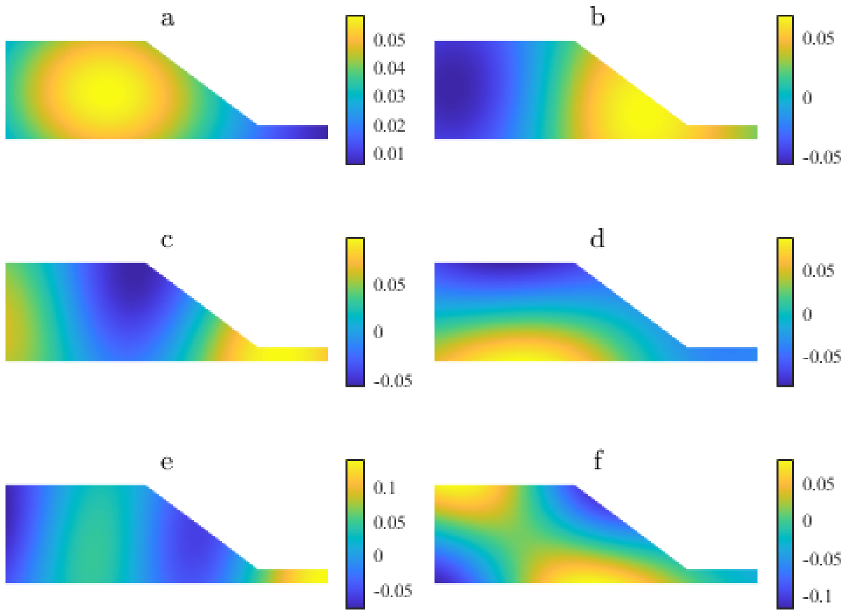

Fig. 5. The first six eigenfunctions of interval fields

in terms of both computational accuracy and efficiency. For the sliding surface 2 of interval field analysis, the interval of f_s is [0.946, 1.132]. Because the interval of the f_s includes one, the slope in this state is unsure. Therefore, it is necessary to increase the lower bound of the f_s though decreasing the angle of the designed slope or enhancing the slope.

Table 2

Results of the efficiency comparison

Method	Result	N
Bayesian optimization	[1.107, 1.415]	21
Surrogate optimization	[1.011, 1.412]	505 + 368

For the same c and φ intervals, the interval field with consideration of spatial uncertainty is compared with the interval analysis method for homogeneous materials. The intervals of f_s were calculated for the interval field and interval analysis, respectively. It can be found in Fig. 8. It can be noticed that the interval field method can reduce the interval of f_s in comparison with the interval analysis method. Moreover, it is

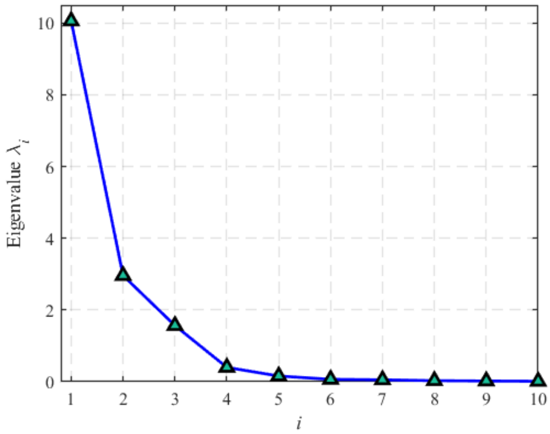

Fig. 6. Eigenvalues of interval fields

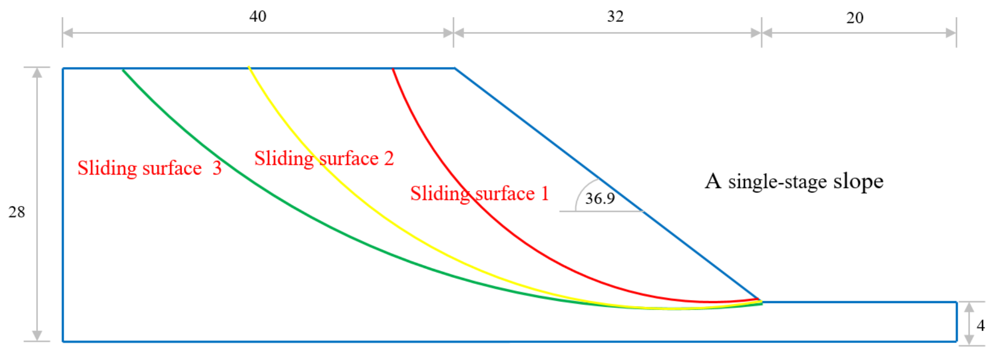

Fig. 7. Three typical sliding surfaces for the single-stage slope failure

more consistent with the real situation after considering the spatial uncertainty.

In order to study the influence of interval field parameters on the calculation results, the influence of spatial dependency length on the calculation results of the interval field is analyzed. It's shown in Figs. 9 and 10. The interval fields were calculated for the horizontal spatial dependency lengths of 5 m, 10 m, 15 , 20 m, 25 m, and 30 m, respectively. The interval fields were calculated for the vertical spatial dependency lengths of 2 m, 4 m, 6 , 8 m, and 10 m, respectively. When the horizontal spatial dependency length is 5 m, the interval of the calculated results is [1.198, 1.341]. And the interval of the calculated results is [1.107, 1.415] when the horizontal spatial dependency length is 30 m. With the expansion of the input parameter interval, the interval of the calculated f_s increases rapidly. When the spatial dependency length is greater

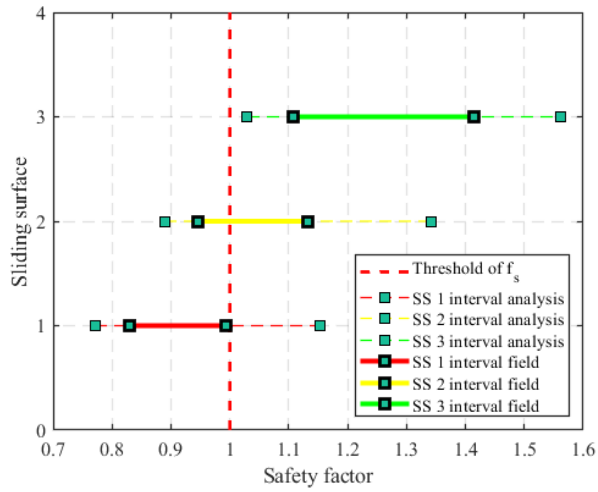

Fig. 8. Results of interval field and interval analysis in the single stage slope analysis

than 25m, the percentage of the interval increase of the f_s becomes larger. Therefore, more attention should be paid to the selection of the spatial dependency length.

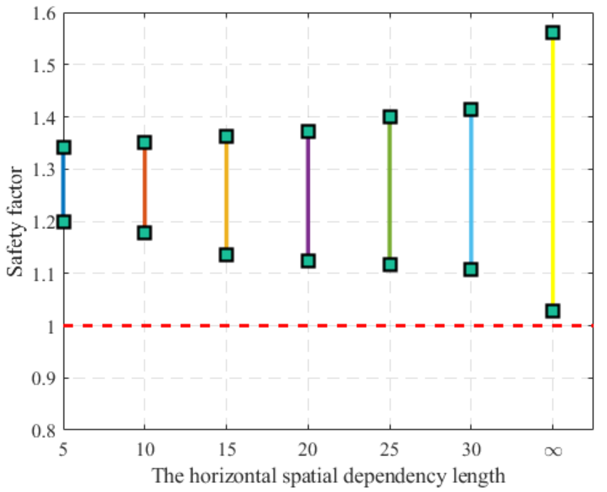

Fig. 9. Influence of the horizontal spatial dependency length on interval field results

In order to explore the influence factors of the interval field, the effect of interval radius is investigated, as shown in Figs. 11 and 12. Fig. 11 shows the effect of c interval radius on the interval field results, and Fig. 12 shows the effect of φ interval radius on the interval field results. For the interval radius of c, the interval field was calculated when it was 1, 2 and 3, respectively. The interval of the calculated results is

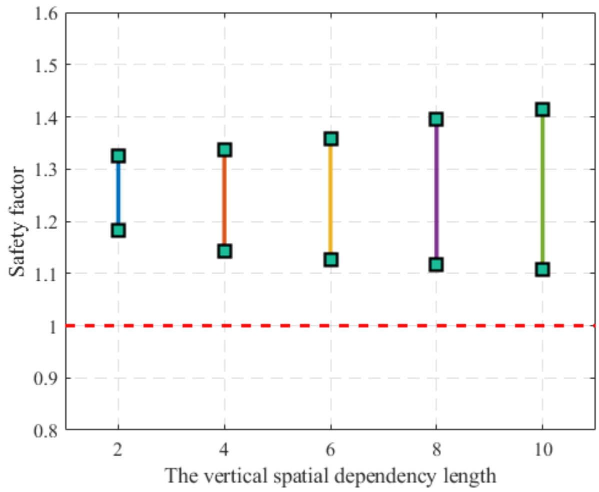

Fig. 10. Influence of the vertical spatial dependency length on interval field results

[1.127, 1.33] when the c interval radius is 1 kPa. When the radius of the c interval is 3 kPa, the interval of the calculated results is [1.107, 1.415]. It is noted that when the radius of the c interval increases, the interval of the f_s also increases. However, the percentage of its increase is small. For the interval radius of φ, the interval field was calculated for its 1, 2, 3, and 4, respectively. When the φ interval radius is 1°, the calculated interval is [1.215, 1.314]. And the interval of the calculated results is [1.107, 1.415] when the radius of the φ interval is 4°. It can be seen that when the radius of the φ interval increases, the interval of the f_s also increases. And the percentage of its increase is larger than the radius of the c interval. It indicates that the φ interval radius has a greater effect on the interval results of the f_s than the c interval radius. Therefore, it can be seen that more attention should be paid to the selection interval radius of the φ. More detailed results can be obtained using interval sensitivity analysis (Moens and Vandepitte, 2007).

5.2. Example 2: Interval field analysis of a two-stage slope

5.2.1. Description of the problem

For illustration, a two-stage slope is used to demonstrate the generation of the interval field, and then the interval of f_s is calculated according to the proposed method. This slope has a lower layer height of 10 m and an upper layer height of 19 m, as shown in Fig. 13. The height of the first slope is 9 m and the angle

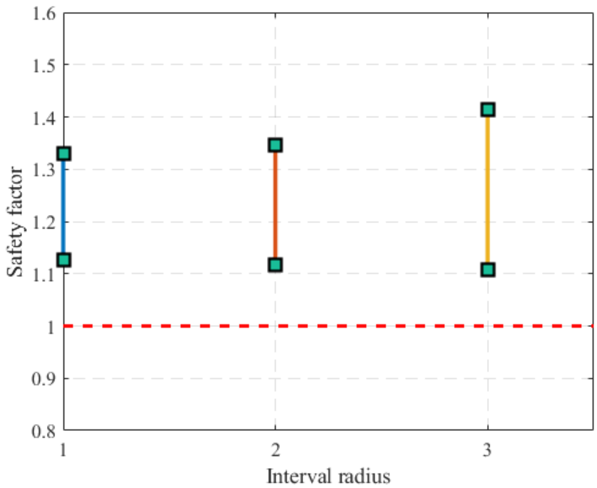

Fig. 11. Influence of cohesive interval radius on interval field results

is 42°. The height of the second slope is 10 m and the angle is 40°. The c interval of the lower layer is [4, 6], the φ interval is [28, 30], and the spatial dependency length is 5 m. The c interval of the upper layer is [10, 12], the φ interval is [28, 36], and both horizontal and vertical spatial dependency lengths are both 5 m. The material parameters are shown in Table 3.

Table 3

Material parameters of the two-stage slope in Example 2

Layers	c(kPa)	φ(°)	l_h	l_h
Lower level	[4, 6]	[24, 26]	5	5
Upper level	[6, 10]	[24, 30]	5	5

5.2.2. Interval field analysis results

First, the interval field of the two-stage slope is generated, as shown in Fig. 14. This figure is a one-time realization of the sample values of the interval field. For this two-stage slope, the generated interval fields are calculated separately for the upper and lower layers. The two-stage slope with interval field is calculated and its slip surface is obtained as shown in Fig. 15. In this figure, three special sliding surfaces are marked. Each type of sliding surface represents a typical picture of the minimum f_s in that region. And each sliding

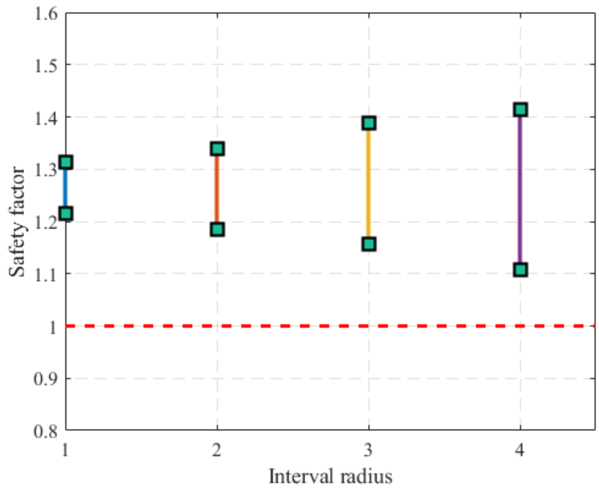

Fig. 12. Influence of the interval radius of the φ on the interval field results

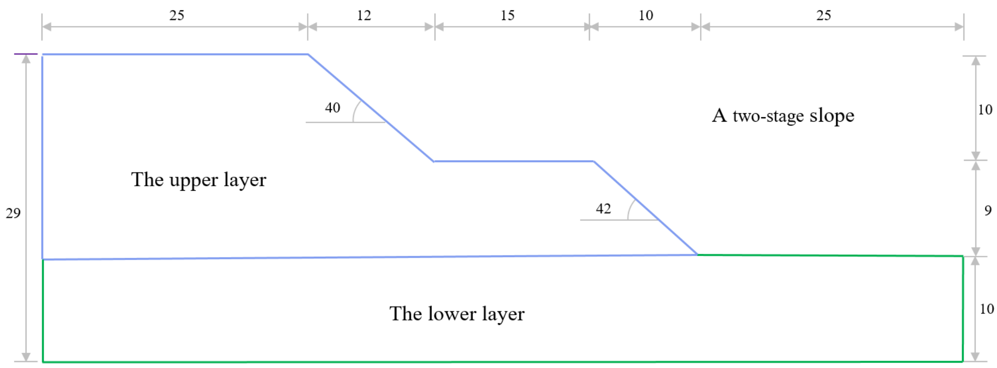

Fig. 13. The geometry model of the two-stage slope

surfaces is analyzed. The interval of f_s was obtained as [1.113, 1.440] for the sliding surface 1, [1.069, 1.117] for the sliding surface 2, and [1.505, 1.529] for the sliding surface 3. The calculated interval of the f_s is represented in Fig. 16.

The intervals of f_s were calculated for the interval field and interval analysis, respectively. The results of the interval limit equilibrium method are compared with those of the interval field limit equilibrium method, as shown in Table 4. It can be noticed that the interval field method can reduce the interval of f_s in comparison with the interval analysis method. And it is obvious that the result of the interval field is larger than 1 so the slope is safe definitely. But the interval analysis lower bound of the f_s at sliding

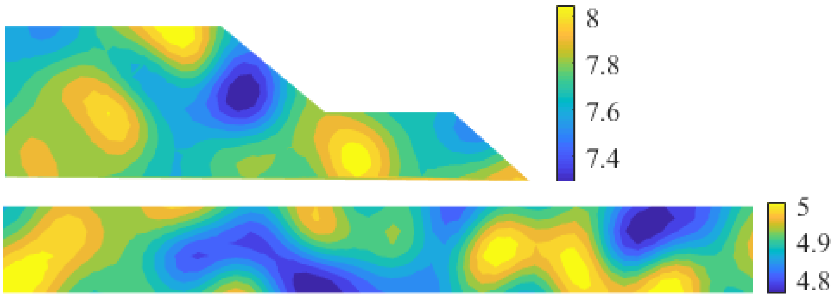

Fig. 14. Sample values realization for the interval field of the two-stage slope

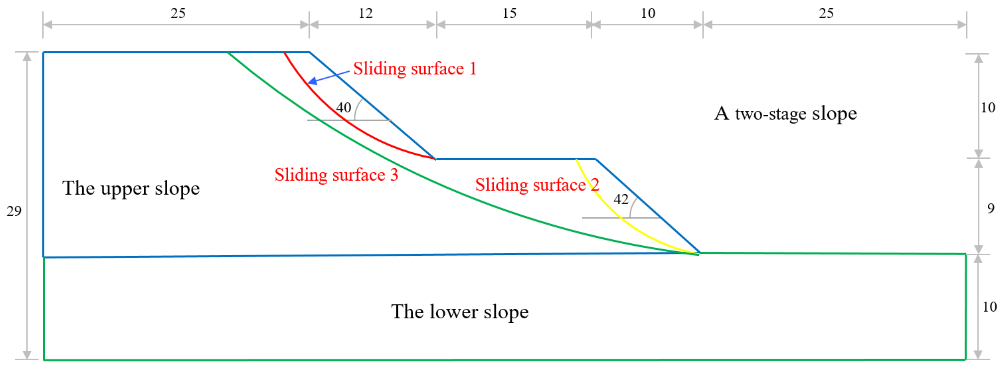

Fig. 15. Three typical sliding surfaces for the two-stage slope failure

surfaces 1 and 2 is less than 1 down to it is unsure in safety state. From this it can be seen that the result of the interval analysis method is more conservative. However, the result of the interval field method is more realistic since it can reflect the spatial uncertainty.

Table 4

Results of interval field in the two-stage slope analysis

Type	Sliding surface 1	Sliding surface 2	Sliding surface 3
Interval field	[1.113, 1.140]	[1.069, 1.117]	[1.505, 1.529]
Interval analysis	[0.953, 1.342]	[0.939, 1.306]	[1.291, 1.719]

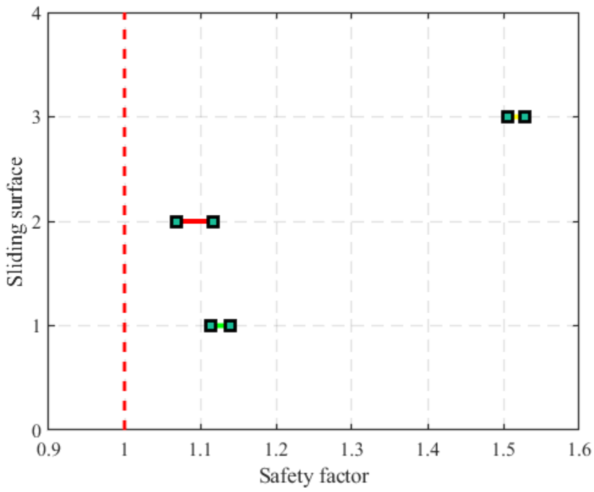

Fig. 16. Results of interval field in the two-stage slope analysis

6. Concluding remarks

The main contribution of this work is the proposal of a new interval field limit equilibrium method, IFLEM, for efficiently estimating the interval of the f_s of a slope in the presence of spatial uncertainty. For our purpose, the IFLEM method first characterizes the interval field by using the Karhunen-Loève like expansion. Further, based on the Morgenstern-Price method and the generated interval field (IF), a computational method for calculating the f_s of slopes is proposed. Then, to efficiently and accurately solve the optimization problem for the upper and lower bounds of the f_s, a dedicated iterative algorithm is developed based on Bayesian global optimization (BGO). Finally, the IFLEM is formed by an elegant combination of IF and LEM. The main feature of IFLEM is the ability to obtain the interval of the f_s, resulting from uncertainties in model parameters and their spatial uncertainty. Two numerical examples are presented to illustrate the availability and effectiveness of the proposed approach. The main concluding remarks includes:

1. The numerical results indicate that the proposed method allows to perform the uncertainty analysis of slopes in the presence of sparse data. Noting that the upper and lower bounds of the f_s are obtained with a small number of deterministic analyses, the proposed method seems to be effective and efficient for quantitative analysis of slopes with scarce data.
2. The influences of the spatial dependency length and the interval radius are investigated. The results shows that different values of spatial dependency length can result in a large variation of the interval of f_s. Besides, compared to the interval radius of c, the interval of f_s is more sensitive to the interval radius of φ. Hence, it is of great significance to reasonably determine the spatial dependency length and the interval radius of φ in the interval field analysis of slopes.
3. The comparison between interval field analysis and interval analysis with homogeneous materials is also performed. Evident differences are observed in the results of the two methods, which implies that the consideration of spatial uncertainty is necessary in the uncertainty quantification of geotechnical engineering structures.

4. Since the deterministic analysis participate the interval field analysis in a decoupled manner, any existing solvers can be easily incorporated into the computational procedure, which makes the method quite general.
5. Due to the high efficiency and generality of the IFLEM, it shows a great potential for the uncertainty quantification of large-scale problems with complicated boundary conditions or practical engineering problems in real world.

Despite the encouraging results of the present study, many further works need to be carried out. In the follow-up study, it is hoped that some advanced slope analysis methods can be incorporated into the proposed method. The consideration of interval reliability analysis methods and interval field expansion methods is another future research effort.

Declaration of competing interest

The authors declare that they have no known competing financial interests or personal relationships that could have appeared to influence the work reported in this paper.

Acknowledgement

This work is supported by the China Scholarship Council (CSC). Chengxin Feng, Chao Dang and Jiashu Yang has received financial support from China Scholarship Council (CSC). Zhibao Zheng is grateful to the Alexander von Humboldt Foundation.

References

Atkinson, K., Han, W., 2009. Numerical solution of fredholm integral equations of the second kind, in: Theoretical Numerical Analysis. Springer, pp. 473–549.

Beer, M., Zhang, Y., Quek, S.T., Phoon, K.K., 2013. Reliability analysis with scarce information: Comparing alternative approaches in a geotechnical engineering context. Structural Safety 41, 1–10.

Callens, R.R.P., Faes, M.G.R., Moens, D., 2021. Local explicit interval fields for non-stationary uncertainty modelling in finite element models. Computer Methods in Applied Mechanics and Engineering 379, 113735.

Cami, B., Javankhoshdel, S., Phoon, K.K., Ching, J., 2020. Scale of Fluctuation for Spatially Varying Soils: Estimation Methods and Values. ASCE-ASME Journal of Risk and Uncertainty in Engineering Systems, Part A: Civil Engineering 6, 03120002.

Catallo, L., 2004. Genetic anti-optimization for reliability structural assessment of precast concrete structures. Computers & Structures 82, 1053–1065.

Chen, Z.Y., Imholz, M., Li, L., Faes, M., Moens, D., 2020. Transient landing dynamics analysis for a lunar lander with random and interval fields. Applied Mathematical Modelling 88, 827–851.

Dang, C., Wei, P., Faes, M.G., Valdebenito, M.A., Beer, M., 2022. Interval uncertainty propagation by a parallel Bayesian global optimization method. Applied Mathematical Modelling 108, 220–235.

Deng, Z., Guo, Z., Zhang, X., 2017. Interval model updating using perturbation method and radial basis function neural networks. Mechanical Systems and Signal Processing 84, 699–716.

Faes, M., Moens, D., 2017. Identification and quantification of spatial interval uncertainty in numerical models. Computers & Structures 192, 16–33.

Faes, M., Moens, D., 2019. Multivariate dependent interval finite element analysis via convex hull pair constructions and the Extended Transformation Method. Computer Methods in Applied Mechanics and Engineering 347, 85–102.

Faes, M., Moens, D., 2020a. On auto- and cross-interdependence in interval field finite element analysis. International Journal for Numerical Methods in Engineering 121, 2033–2050.

Faes, M., Moens, D., 2020b. Recent trends in the modeling and quantification of non-probabilistic uncertainty. Archives of Computational Methods in Engineering 27, 633–671.

Faes, M.G., Broggi, M., Spanos, P.D., Beer, M., 2022. Elucidating appealing features of differentiable auto-correlation functions: A study on the modified exponential kernel. Probabilistic Engineering Mechanics , 103269.

Griffiths, D.V., Fenton, G.A., 2004. Probabilistic Slope Stability Analysis by Finite Elements. Journal of Geotechnical and Geoenvironmental Engineering 130, 507–518.

Han, Z.H., Görtz, S., 2012. Hierarchical Kriging Model for Variable-Fidelity Surrogate Modeling. AIAA Journal 50, 1885–1896. Publisher: American Institute of Aeronautics and Astronautics.

Huang, S., Quek, S., Phoon, K., 2001. Convergence study of the truncated Karhunen-Loève expansion for simulation of stochastic processes. International Journal for Numerical Methods in Engineering 52, 1029–1043.

Jiang, S.H., Huang, J., Griffiths, D., Deng, Z.P., 2022. Advances in reliability and risk analyses of slopes in spatially variable soils: A state-of-the-art review. Computers and Geotechnics 141, 104498.

Jones, D.R., Schonlau, M., Welch, W.J., 1998. Efficient Global Optimization of Expensive Black-Box Functions. Journal of Global Optimization 13, 455–492.

Liu, S., Shao, L., Li, H., 2015. Slope stability analysis using the limit equilibrium method and two finite element methods. Computers and Geotechnics 63, 291–298.

Länsivaara, T., Phoon, K.K., Ching, J., 2021. What is a characteristic value for soils? Georisk: Assessment and Management of Risk for Engineered Systems and Geohazards , 1–26.

Moens, D., De Munck, M., Desmet, W., Vandepitte, D., 2011. Numerical dynamic analysis of uncertain mechanical structures based on interval fields, in: IUTAM symposium on the vibration analysis of structures with uncertainties, Springer. pp. 71–83.

Moens, D., Hanss, M., 2011. Non-probabilistic finite element analysis for parametric uncertainty treatment in applied mechanics: Recent advances. Finite Elements in Analysis and Design 47, 4–16.

Moens, D., Vandepitte, D., 2007. Interval sensitivity theory and its application to frequency response envelope analysis of uncertain structures. Computer Methods in Applied Mechanics and Engineering 196, 2486–2496.

Montoya-Noguera, S., Zhao, T., Hu, Y., Wang, Y., Phoon, K.K., 2019. Simulation of non-stationary non-Gaussian random fields from sparse measurements using Bayesian compressive sampling and Karhunen-Loève expansion. Structural Safety 79, 66–79.

Morgenstern, N.u., Price, V.E., 1965. The analysis of the stability of general slip surfaces. Geotechnique 15, 79–93.

Ni, B.Y., Jiang, C., 2020. Interval field model and interval finite element analysis. Computer Methods in Applied Mechanics and Engineering 360, 112713.

Ni, B.Y., Jiang, C., Han, X., 2016. An improved multidimensional parallelepiped non-probabilistic model for structural uncertainty analysis. Applied Mathematical Modelling 40, 4727–4745.

Phoon, K.K., Kulhawy, F.H., 1999a. Characterization of geotechnical variability. Canadian Geotechnical Journal 36, 612–624. Publisher: NRC Research Press.

Phoon, K.K., Kulhawy, F.H., 1999b. Evaluation of geotechnical property variability. Canadian Geotechnical Journal 36, 625–639.

Rubinstein, R.Y., Kroese, D.P., 2016. Simulation and the Monte Carlo method. John Wiley & Sons.

Sofi, A., 2015. Structural response variability under spatially dependent uncertainty: stochastic versus interval model. Probabilistic Engineering Mechanics 42, 78–86.

Sofi, A., Muscolino, G., Elishakoff, I., 2015. Static response bounds of Timoshenko beams with spatially varying interval uncertainties. Acta Mechanica 226, 3737–3748.

Sofi, A., Romeo, E., Barrera, O., Cocks, A., 2019. An interval finite element method for the analysis of structures with spatially varying uncertainties. Advances in Engineering Software 128, 1–19.

Spanos, P.D., Beer, M., Red-Horse, J., 2007. Karhunen-Loève expansion of stochastic processes with a modified exponential covariance kernel. Journal of Engineering Mechanics 133, 773–779.

Wang, C., Qiu, Z., Wang, X., Wu, D., 2014. Interval finite element analysis and reliability-based optimization of coupled structural-acoustic system with uncertain parameters. Finite Elements in Analysis and Design 91, 108–114.

Wang, Y., Zhao, T., Phoon, K.K., 2019. Statistical inference of random field auto-correlation structure from multiple sets of incomplete and sparse measurements using Bayesian compressive sampling-based bootstrapping. Mechanical Systems and Signal Processing 124, 217–236.

Zhu, D.Y., Lee, C.F., Qian, Q.H., Chen, G.R., 2005. A concise algorithm for computing the factor of safety using the morgenstern-price method. Canadian Geotechnical Journal 42, 272–278.